PAPER

Atomistic aspects of $\frac{1}{2}\langle 1\,1\,1\rangle$screw dislocation behavior in α-iron and the derivation of microscopic yield criterion

To cite this article: Z M Chen *et al* 2013 *Modelling Simul. Mater. Sci. Eng.* **21** 055023

Modelling Simul. Mater. Sci. Eng. **21** (2013) 055023 (18pp) doi:10.1088/0965-0393/21/5/055023

Atomistic aspects of $\frac{1}{2}\langle 1\,1\,1\rangle$ screw dislocation behavior in α-iron and the derivation of microscopic yield criterion

Z M Chen[1], **M Mrovec**[1,2] **and P Gumbsch**[1,2]

[1] Institute for Applied Materials IAM, Karlsruhe Institute of Technology, 76131 Karlsruhe, Germany
[2] Fraunhofer Institute for Mechanics of Materials IWM, Wöhlerstr. 11, 79108 Freiburg, Germany

E-mail: matous.mrovec@iwm.fraunhofer.de

Received 7 February 2013, in final form 14 May 2013
Published 24 June 2013
Online at stacks.iop.org/MSMSE/21/055023

Abstract
The plastic deformation of body-centered cubic iron at low temperatures is governed by slip behavior of $\frac{1}{2}\langle 1\,1\,1\rangle$ screw dislocations. Their non-planar core structure gives rise to a strong temperature dependence of the yield stress and overall plastic behavior that does not follow the Schmid law common to most close-packed metals. In this work,we carry out a systematic study of the screw dislocation behavior in α-Fe by means of atomistic simulations using a state-of-the-art magnetic bond-order potential. Based on the atomistic simulations of the screw dislocations under various external loadings, we formulate an analytical yield criterion that correctly captures the non-Schmid plastic response of iron single crystals under general loading conditions. The theoretical predictions of operative slip systems for uniaxial loadings agree well with available experimental observations, and demonstrate the robustness and reliability of such atomistically based yield criterion. In addition, this bottom-up approach can be directly utilized to formulate dislocation mobility rules in mesoscopic discrete dislocation dynamics simulations.

(Some figures may appear in colour only in the online journal)

1. Introduction

It has been established by a number of experimental and theoretical studies (for reviews, see [1–6]) that the low-temperature plastic behavior of body-centered cubic (bcc) metals including α-Fe does not follow the Schmid law [7], which is commonly used to describe the plastic flow of face-centered cubic (fcc) metals. The breakdown of the Schmid law in bcc metals is the consequence of the non-planar core structure and associated high lattice friction of the $\frac{1}{2}\langle 1\,1\,1\rangle$ screw dislocations [8, 9]. In order to comprehend the macroscopic plasticity of bcc

iron, it is therefore essential to thoroughly understand the behavior of the screw dislocations at the nanoscale.

Linking the properties of a single dislocation at the atomic scale with the plastic response of macroscopic crystal is a challenging task that requires a consistent employment of different modelling approaches across a broad range of length and time scales. At the atomic level, it is necessary not only to examine the intrinsic properties of the dislocation at the equilibrium but especially how the dislocation responds to externally applied loads. The purpose is to identify the components of the stress tensor that influence the motion of an individual screw dislocation, and subsequently to quantify their effects on the magnitude of the Peierls stress. It has been revealed by several atomistic studies [8, 10, 11] that the glide of the screw dislocation in bcc metals is significantly affected by stress components other than those parallel to the slip direction. These so-called non-Schmid stresses do not exert any force on the dislocation, but can change both the Peierls stress and the glide plane by altering the dislocation core structure. Direct manifestations of these atomic-scale phenomena are experimentally observed twinning–antitwinning and tension–compression asymmetries [3].

The results of atomistic studies can be incorporated into mesoscopic computational approaches such as the discrete dislocation dynamics (DDD) [12, 13] that can study ensembles containing many dislocations for time scales much longer than those accessible in atomistic simulations. The crucial inputs for DDD methods are dislocation mobility rules. While these rules are relatively straightforward for edge and mixed dislocations with planar cores, whose motion is confined to a particular glide plane and affected primarily by phonon drag [14, 15], the prescriptions for screw dislocation mobilities have so far relied mostly on empirical models based on macroscopic materials behavior [12, 16]. However, the screw dislocations move by a thermally activated nucleation of pairs of kinks [17, 18], and their mobilities are determined by the activation enthalpy associated with this process. The activation enthalpy is not a constant but depends on the local stress state along the dislocation, i.e. it also reflects the changes in the Peierls stress and associated Peierls barrier due to non-Schmid effects. Full atomistic descriptions of the screw dislocation mobilities that take into account the non-Schmid behavior have been attempted only very recently [19–21].

Apart from explicit DDD simulations, continuum yield criteria are highly desirable for macroscopic engineering calculations. With such yield criterions the microscopic behavior can be represented using a small number of fundamental parameters. The early framework of the continuum description for single crystal plasticity was developed by Hill [22] and Rice [23] based on the Schmid law for fcc metals. The first systematic work on the non-Schmid description was carried out in the early 1990s by Qin and Bassani [24, 25] who constructed a simple form of an effective yield criterion in which the yield stress is written as a linear combination of both the Schmid and non-Schmid stresses. Based on these studies, Vitek *et al* [19, 26] and Gröger *et al* [20] formulated a general form of the yield criterion for the non-associated flow in bcc metals that can describe the commencement of the motion of the $\frac{1}{2}\langle 1\,1\,1\rangle$ screw dislocations under general external loading. This yield criterion was shown to reproduce closely the atomistic results including the twinning–antitwinning and tension–compression asymmetries.

In this work, we systematically investigate the intrinsic properties of the $\frac{1}{2}\langle 1\,1\,1\rangle$ screw dislocation in α-Fe using a recently developed magnetic bond-order potential (BOP) [27]. Our study builds on and further extends existing analyses of the screw dislocation behavior in non-magnetic bcc metals [11, 28, 29]. We focus first on the effect of the pure shear stress parallel to the Burgers vector to demonstrate the dependence of the critical resolved shear stress (CRSS) on the sense and orientation of the shearing and to reveal the twinning–antitwinning asymmetry observed in experiments [3, 8]. We then determine the CRSS for the screw dislocation under

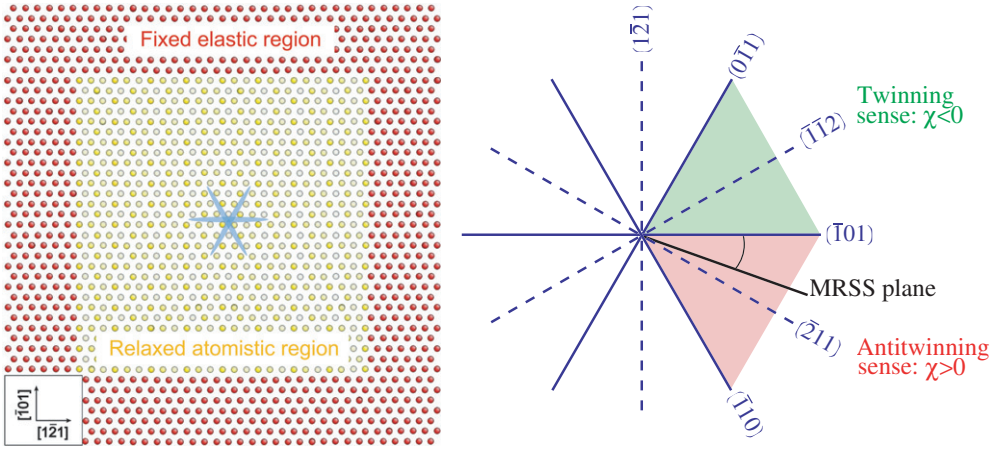

Figure 1. Schematic picture of the simulation block and orientation of the planes in the [1 1 1] zone.

uniaxial loadings in tension and compression to compare with the experimentally observed tension–compression asymmetry [3]. These calculations also reveal whether the shear stress parallel to the slip direction, which exerts the Peach–Köhler force to drive the dislocation, is the only stress component controlling the motion of the dislocation or whether other components of the stress tensor, e.g. the shear stresses perpendicular to the Burgers vector, also affect the dislocation motion in iron. The results enable us to explain the anomalous slip observed in experiments, and to analyse in detail how the CRSS is influenced by the changes in the non-planar core structure of the $\frac{1}{2}\langle 1\,1\,1\rangle$ screw dislocation.

Based on the atomistic results,we formulate an analytical yield criterion that can predict the slip behavior of α-Fe single crystals in arbitrary loading orientation. This criterion extends previous formulations [20] to closely reproduce the atomistic data not only for the glide on the primary slip system but also for cases of anomalous slip. This bottom-up methodology can also be utilized for transparent and physically based parametrization of mobility rules in DDD modeling schemes. A first such implementation has been recently elaborated for W [30] and α-Fe [31].

2. Methodology

In this work, we employ a magnetic BOP for iron [27], which was shown to reliably describe not only the equilibrium core structure of the $\frac{1}{2}\langle 1\,1\,1\rangle$ screw dislocation in α-Fe but also its behavior under applied stress. The magnetic BOP is based on the tight-binding approximation and is able to capture the angular character of unsaturated chemical bonds in the middle transition metals originating from the d-electrons. The BOP model also includes a physically based description of magnetic contributions via the Stoner model of itinerant magnetism and correctly reproduces the relative stability of different magnetic bulk phases as well as changes of local magnetic moments in the vicinity of lattice defects. Despite its quantum mechanical origin, the real space BOP formalism is computationally efficient and not limited by the periodic boundary conditions. This makes it particularly suitable for modeling of extended defects.

The simulation block used in our calculations is depicted schematically in figure 1. The rectangular block is periodic along the z-direction, which coincides with the [1 1 1] direction of the dislocation line. The periodic length of the block in the z direction equals the Burgers

vector $b = \sqrt{3}/2a_0$ ($a_0 = 2.85$ Å is the lattice parameter). Therefore, the dislocation in our simulations is always straight and infinite without any kinks or jogs. The $\frac{1}{2}\langle 1\,1\,1\rangle$ screw dislocation is introduced in the center of the block by displacing the atoms according to the anisotropic elastic displacement field in an infinite medium [32]. The y- and x-axes of the block are perpendicular to the $(\bar{1}\,0\,1)$ and $(\bar{1}\,2\,\bar{1})$ planes, respectively. Fixed boundary conditions are used along these directions so that the dislocation is effectively placed in an infinite crystal environment during the whole simulation. The dimensions of the block in the x- and y-directions are about 20×20 lattice parameters, which was tested to be large enough for a single screw dislocation. The atomic positions in the active region of the block were fully relaxed while those in the boundary region were fixed to maintain the elastic field of the screw dislocation in an infinite medium. The relaxation was considered complete when the forces on all atoms fell below 0.001 eV Å^{-1}. In all our calculations, the fast inertial relaxation engine (FIRE) algorithm [33] was employed to carry out the atomic relaxations.

In simulations of the dislocation under external loading, an elastic displacement field corresponding to the applied stress is superimposed on the whole simulation block. The stress is built up incrementally in steps of $0.0005C_{44}$, where C_{44} is the shear elastic modulus. The relaxation is carried out after each stress increment.

3. Atomistic studies

The BOP model predicts that the $\frac{1}{2}[1\,1\,1]$ screw dislocation spreads symmetrically on the three $\{1\,1\,0\}$ planes of the $[1\,1\,1]$ zone adopting the so-called non-degenerate core structure [27], virtually identical to that found in DFT calculations [34, 35]. The main purpose of this study is to identify the stress components affecting the glide of the screw dislocation, and, subsequently, to quantify their effects on the magnitude of the Peierls stress. In order to analyze these phenomena, we investigated the behavior of the dislocation under three distinct loading conditions:

(i) loading by pure shear stress parallel to the slip direction on different maximum resolved shear stress planes (MRSSP);
(ii) uniaxial loading in tension and compression;
(iii) loading using a reduced stress tensor containing only two shear stress components parallel and perpendicular to the slip direction.

Results of these simulations are described in the following subsections.

3.1. Loading by pure shear stress parallel to the slip direction

The loading with pure shear stress, which cannot easily be applied in experiments, provides the simplest and most direct way to obtain the Peierls stress. This pure shear stress loading was applied to different MRSSPs using the stress tensor:

$$\Sigma_\sigma = \begin{bmatrix} 0 & 0 & 0 \\ 0 & 0 & \sigma \\ 0 & \sigma & 0 \end{bmatrix}. \tag{1}$$

This stress tensor is defined in the right-handed coordinate system with the y-axis normal to the MRSSP, the z-axis parallel to the $[1\,1\,1]$ direction, and the x-axis lying in the MRSSP. As illustrated in figure 1, the orientation of the MRSSP is described by the angle χ with respect to the reference $(\bar{1}\,0\,1)$ plane. Owing to the lattice symmetry, it is sufficient to consider the range $-30^\circ \leqslant \chi \leqslant 30^\circ$. In our calculations, the positive stress σ applied on MRSSPs within

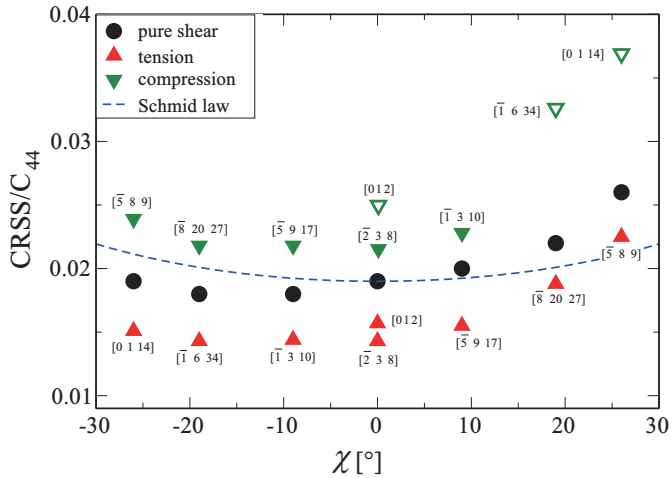

Figure 2. Magnitudes of CRSSs as a function of the MRSSP orientation and the type of loading (black circles: pure shear; red up-triangles: tension; green down-triangles: compression). According to the Schmid law, the CRSS should not depend on the orientation of the MRSSP therefore be proportional to $\cos^{-1}\chi$ (dashed line).

$0^\circ \leqslant \chi \leqslant 30^\circ$, i.e. bounded by the $(\bar{2}11)$ and $(\bar{1}\,0\,1)$ planes, corresponds to shearing in the antitwinning sense while for MRSSPs within $-30^\circ \leqslant \chi \leqslant 0^\circ$, i.e. bounded by the $(\bar{1}\,\bar{1}\,2)$ and $(\bar{1}\,0\,1)$ planes, the shearing is in the twinning sense.

According to our simulations, the dislocation glides exclusively on the $(\bar{1}\,0\,1)$ plane for all pure shear loadings. The calculated dependence of the CRSS on the orientation of the MRSSP is plotted by full circles in figure 2. The predicted CRSS-χ dependence for α-Fe clearly deviates from the Schmid law that is shown by a dashed line. The orientations with positive and negative χ are not equivalent, and the CRSS is higher when the crystal is loaded in the antitwinning sense (positive χ values) than in the twinning sense (negative χ values).

As the shear stress increases, the dislocation core gradually transforms from its symmetric non-degenerate configuration to a less symmetric form. Figure 3(*a*) shows the distortions of the differential displacements [36] in the core under pure shear stress applied on the $(\bar{1}\,0\,1)$ plane is equal to $0.015C_{44}$ (i.e. about 75% of the Peierls stress). We see that there is a marked reduction on the left and a large increase on the right of the dislocation center, which correspond to the shift of the Burgers vector from the original core position towards the neighboring lattice site. The symbols in figure 3(*a*) also clearly reveal the twinning–antitwinning effect. The change of the core is not symmetric above and below the $(\bar{1}\,0\,1)$ glide plane. The core preferentially extends in the twinning region while it contracts in the anti-twinning region (see figure 1).

3.2. Loading in tension and compression

Loadings in tension and compression disclose whether or not the shear stress parallel to the slip direction is the only stress component affecting the dislocation motion. Since such uniaxial loading is also a preferred experimental testing geometry, simulation results can be compared directly to experimental data.

The uniaxial loading orientations investigated in our study are shown in figure 4 as solid circles. For each of these orientations the MRSSP corresponds to an MRSSP which is used

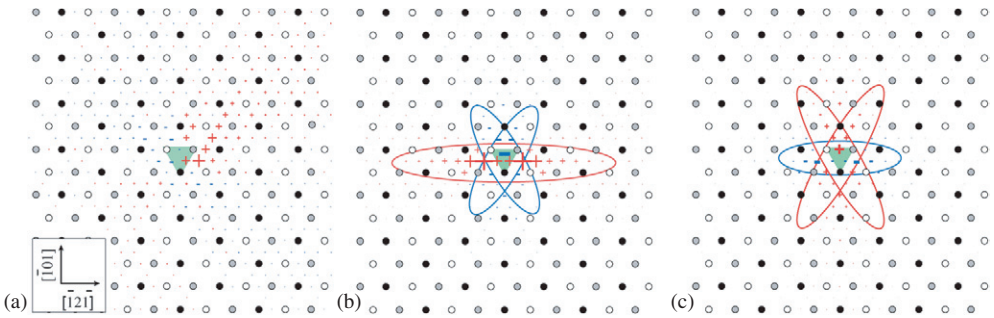

Figure 3. Changes of the differential displacements around the core under pure shear stress is equal to $0.015C_{44}$ applied parallel to the Burgers vector on the $(\bar{1}\,0\,1)$ plane (a), and non-Schmid stresses applied perpendicular to the Burgers vector with $\tau = +0.02C_{44}$ (b) and $\tau = -0.02C_{44}$ (c). The plus and minus symbols correspond to the increase and decrease of the differential displacements, respectively. The green triangle marks the initial position of the dislocation center.

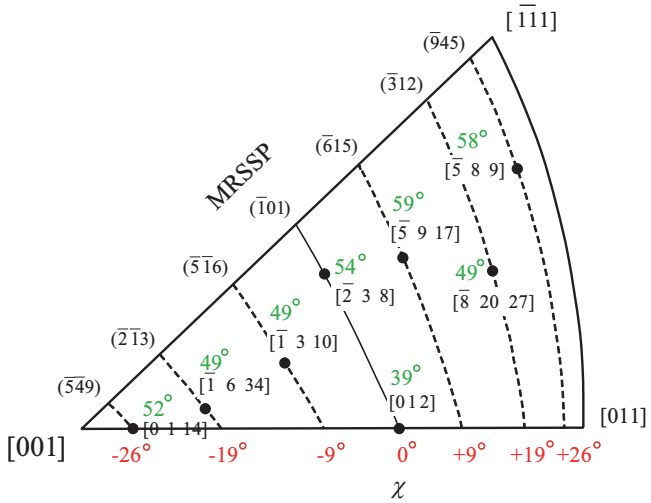

Figure 4. Standard stereographic triangle for which the $(\bar{1}\,0\,1)$ plane is the most highly stressed $\{1\,1\,0\}$ plane in the [1 1 1] zone. Uniaxial loading orientations investigated in this work are marked by black circles and their corresponding MRSSPs are given in parentheses. The angles χ and λ (the angle between the loading orientation and the Burgers vector) are displayed in red and green, respectively.

in the previous section for the pure shear loadings (marked by dashed lines). One should note that with the same loading direction the sign of the shear stress component parallel to the slip direction is reversed for tension and compression. It means that when comparing the compression results with those of tension, the sign of χ should be reversed as well.

The CRSS values from the uniaxial loading projected on the MRSSP parallel to the [1 1 1] direction can be compared with the CRSS determined from pure shear loading presented in the previous section. If the two critical stresses are not the same, the glide of the screw dislocation must be affected by other components of the stress tensor.Our results displayed as triangles in figure 2 show that this is indeed the case. For a given χ, the CRSS for compression is always considerably higher than that for tension, while the value for the pure shear loading (circles) lies in between. The non-glide stress components therefore make it easier for the screw dislocation to glide in tension and harder in compression.

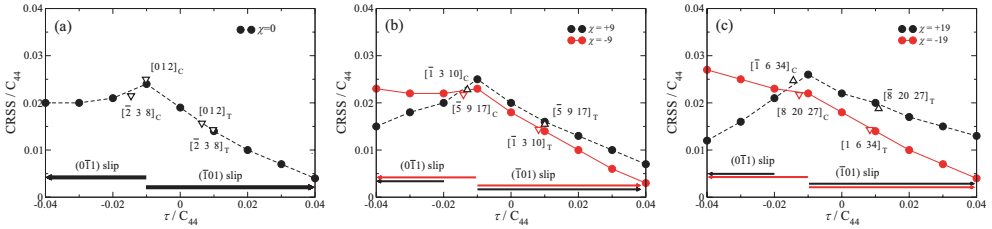

Figure 5. Dependence of the CRSS on the shear stress perpendicular to the slip direction for different MRSSPs: (*a*) $\chi = 0$, (*b*) $\chi = \pm 9$ and (*c*) $\chi = \pm 19$. The triangles correspond to the uniaxial loading results calculated in section 3.2.

For loading in tension, the screw dislocation glides exclusively on the $(\bar{1}\,0\,1)$ plane as under pure shear. However, for most loading directions in compression (the solid upside down triangles in figure 2) the glide plane changed from $(1\,0\,\bar{1})$ to $(1\,\bar{1}\,0)$ although the Schmid factor is two times higher on the former slip system. This shows that the changes of the dislocation core due to the non-Schmid stresses affect not only the Peierls stress but also the preferred glide plane. The empty triangles in figure 2 present special cases. For the [0 1 2] compression ($\chi = 0$), the dislocation glides seemingly on the $(2\bar{1}\,\bar{1})$ plane. However, this motion is still composed of alternating jumps on two $\{1\,1\,0\}$ glide planes and no direct jump of the screw dislocation along the $(2\bar{1}\,\bar{1})$ plane takes place. For compression loading with large positive χ values of $+19^\circ$ and $+26^\circ$, the dislocation core effectively splits along the inclined $(1\bar{1}\,0)$ plane and the Peierls stress becomes excessively large. As will be discussed later, other slip systems will be activated in real crystals before such high stresses are reached.

3.3. Loading by shear stresses parallel and perpendicular to the slip direction

Previous atomistic studies on bcc metals [9–11, 19, 26] have shown that the most relevant non-Schmid stresses are the shear stresses perpendicular to the slip direction, but there are indications that normal stresses may also influence dislocation behavior [37]. In order to investigate the dependence of the CRSS on the magnitude of the shear stress perpendicular to the slip direction, we carried out a set of simulations of the $\frac{1}{2}[1\,1\,1]$ screw dislocation subjected to simultaneous loading by various combination of shear stresses parallel and perpendicular to the slip direction using the following stress tensor:

$$\Sigma_{\tau,\sigma} = \begin{bmatrix} -\tau & 0 & 0 \\ 0 & \tau & \sigma \\ 0 & \sigma & 0 \end{bmatrix}. \tag{2}$$

This stress tensor is similar to that in equation (1) except for the presence of the additional diagonal stress components $\pm\tau$, which represent the shear stresses perpendicular to the [1 1 1] direction in the coordinate system rotated by -45° around the z-axis. Such a reduction in the general stress tensor presents a convenient simplification of the general loading conditions that can readily reveal the crucial effect of the two perpendicular shear stresses.

Figure 5 shows the computed dependences of the CRSS on the shear stress τ for five MRSSP orientations with $|\chi| < 20^\circ$ together with results from corresponding uniaxial loading simulations described in the previous section. For all five investigated orientations, the CRSS is lower for positive τ than for $\tau = 0$, and in this region the dislocation always glides on the $(\bar{1}\,0\,1)$ plane. In contrast, negative τ makes the glide on the $(\bar{1}\,0\,1)$ plane more difficult. Furthermore, in the region of negative τ the CRSS increases with decreasing τ until the glide plane changes

from the $(\bar{1}\,0\,1)$ plane to the $(0\,\bar{1}\,1)$ plane. The operating glide planes are indicated by the bars in the bottom of figure 5. In the vicinity of the transition, both slip systems are likely to become activated, resulting in a macroscopic glide along the $(\bar{1}\,\bar{1}\,2)$ plane or some other high-index plane. These results are fully consistent with those from the corresponding uniaxial loading simulations (labeled as triangles), where the shear stress τ perpendicular to the slip direction and its corresponding CRSS were extracted from the deviatoric part of the stress tensor.

3.4. Discussion of atomistic results

The results of our atomistic simulations show that the CRSS of the $\frac{1}{2}[1\,1\,1]$ screw dislocation depends predominantly on just two factors: the orientation of the slip system given by χ, and the non-Schmid shear stresses given by τ. The underlying microscopic mechanisms responsible for this behavior are linked to changes of the dislocation core.

For pure shear stress parallel to the Burgers vector, i.e. without any non-Schmid stresses, the dislocation core gradually transforms from its symmetric non-degenerate configuration [27, 35] to a less symmetric form as the loading increases. It has usually been assumed [11] that during the glide the 'arms' on the inclined $\{1\,1\,0\}$ planes shorten while those on the most stressed $(\bar{1}\,0\,1)$ plane become more extended, rendering the core more glissile. Figure 3(*a*) showing the changes of the differential displacements around the core under pure shear stress reveals that this assumption is not completely correct. We see that the largest changes of the core indeed occur on the horizontal $(\bar{1}\,0\,1)$ glide plane, but they are limited to the very core center only: there is a marked reduction on the left from the initial position and a large increase on the right at the final position. This corresponds to the shift of the Burgers vector from the original core position to the neighboring stable site. The symbols in figure 3(*a*) also clearly reveal the twinning–antitwinning effect in the bcc lattice. Although the pure shear stress parallel to the slip direction is applied along the horizontal $(\bar{1}\,0\,1)$ plane, which is a mirror plane, the change of the core is not symmetric about this plane. The core under stress prefers to extend more in the twinning region above the $(\bar{1}\,0\,1)$ plane $(-60^\circ < \chi < 0^\circ)$, while it contracts in the anti-twinning region below the $(\bar{1}\,0\,1)$ plane $(-0^\circ < \chi < 60^\circ)$. This also explains the twinning–antitwinning asymmetry obtained for the CRSS versus χ.

Apart from the pure shear stress calculations, we also showed in figure 2 that for a given loading direction the CRSS for tension is always lower than that for compression. This tension–compression asymmetry clearly indicates that the CRSS depends not only on the Schmid stress, but also on stresses other than those parallel to the slip direction. In agreement with most previous studies [10, 11, 19, 37], the glide of the screw dislocation is affected most by the shear stress perpendicular to the slip direction. Although this stress component does not directly drive the screw dislocation to move, it changes the symmetry of the core and makes the dislocation either easier or harder to slip on different $\{1\,1\,0\}$ planes. Examples of core changes for two different stresses τ are displaced in figures 3(*b*) and (*c*). For positive τ, the dislocation core extends along the $(\bar{1}\,0\,1)$ plane and constricts on both $(0\,\bar{1}\,1)$ and $(\bar{1}\,1\,0)$ planes resulting in an easier glide on the $(\bar{1}\,0\,1)$ plane. On the other hand, for negative τ, the core constricts along the $(\bar{1}\,0\,1)$ plane and extends on both $(0\,\bar{1}\,1)$ and $(\bar{1}\,1\,0)$ planes. If these extensions are large enough, it may become more favorable for the dislocation to move on the low stressed $(0\,\bar{1}\,1)$ or $(\bar{1}\,1\,0)$ planes than on the primary $(\bar{1}\,0\,1)$ glide plane. The analysis is fully in accordance with results in figure 5. The CRSS is lower for $\tau > 0$ than for $\tau = 0$, and in the region of positive τ the dislocation always glides on the $(\bar{1}\,0\,1)$ plane. In contrast, negative τ makes the glide on the $(\bar{1}\,0\,1)$ plane more difficult. With decreasing τ the CRSS increases until the glide

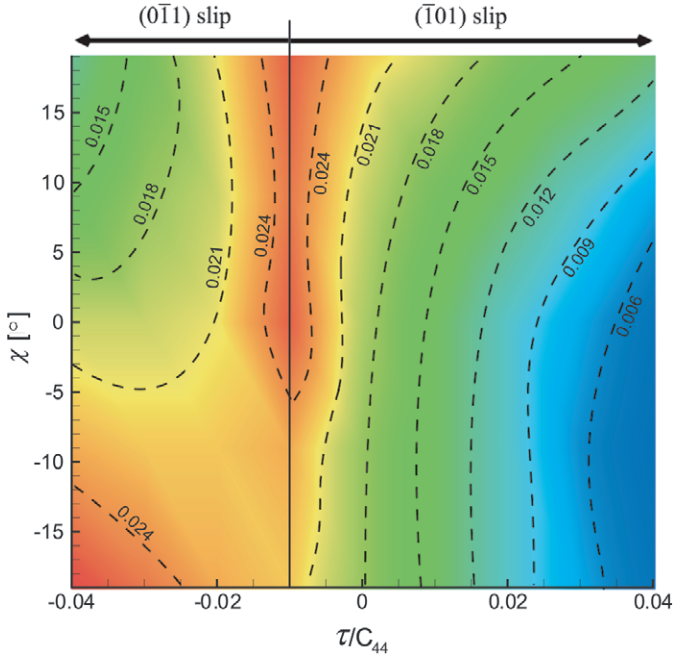

Figure 6. The dependence of CRSS on the MRSSP angle χ and the shear stress τ perpendicular to the slip direction.

plane changes from the $(\bar{1}\,0\,1)$ plane to the $(0\,\bar{1}\,1)$ plane. In situations when both slip systems may be activated simultaneously (for $\tau \approx -0.01C_{44}$), the motion of the screw dislocation is composed of alternating jumps on both slip systems so that the apparent macroscopic slip takes place on the $(\bar{1}\,\bar{1}\,2)$ plane. Additionally, extensive experimental evidence exists for non-crystallographic slip or slip on high index planes for certain uniaxial loadings in pure single crystals of iron and other refractory metals [3, 17, 38, 39]. This macroscopic phenomenon originates from stochastic transitions between the neighboring $\{1\,1\,0\}$ slip systems and is discussed elsewhere [31]. It should be stressed here that the elementary slip at the microscopic level takes place exclusively on the $\{1\,1\,0\}$ planes in agreement with experimental observations [40–43].

In contrast to a recent theoretical study by Koester *et al* [37], we did not find any significant influence of the normal stresses on the screw dislocation mobility. A possible reason behind this difference is the application of a less sophisticated interatomic potential in their simulations that is known to be less reliable when describing the dislocation behavior under applied stress [27, 44]. The role of normal stresses should therefore be reexamined, preferably by accurate electronic structure methods.

Figure 6 summarizing the dependence of the CRSS on both χ and τ is the major outcome of the atomistic calculations. The color shading in this contour graph represents the change of the CRSS from low (blue) to high (red). Additionally, the plot is divided into two regions, each corresponding to a different glide plane.

In the right part of the plot the glide plane is $(\bar{1}\,0\,1)$. In this region, the CRSS decreases with increasing τ for all MRSSP orientations due to the effect of the shear stress perpendicular to the slip direction. In the vertical direction, the variations of the CRSS at constant τ are governed by the twinning–antitwinning asymmetry and the Schmid factor.

In the region where $(\bar{1}\,0\,1)$ slip prevails, the CRSS varies strongly only in the antitwinning zone ($\chi > 0$) while it remains almost constant in the twinning zone ($\chi < 0$). This result is consistent with experimentally observed twinning–antitwinning asymmetry in iron single crystals deformed at very low temperatures [40]. The sharp increase on the antitwinning side can be qualitatively explained by the simultaneous increase of the Schmid factor and the rotation of the MRSSP towards the 'hard' antitwinning $(\bar{2}\,1\,1)$ plane. For negative χ values, the effect of increasing Schmid factor is compensated by rotation of the MRSSP towards the 'easy' twinning $(\bar{1}\,\bar{1}\,2)$ plane so that CRSS remains almost constant in this region.

The analysis of the left part of figure 6 for negative τ is similar but more complex. For the CRSS the competition occurs mainly between the effects of the Schmid factor and the shear stress perpendicular to the slip direction. On one hand, as χ decreases from $+19^\circ$ to -19° the Schmid factor increases on the $(0\,\bar{1}\,1)$ plane, indicating that the CRSS should decrease for a constant τ. On the other hand, as χ decreases the core extension along the glide plane is gradually reduced. This constriction has an opposite effect than the Schmid factor leading to an increase of CRSS with decreasing χ. For larger negative values of τ ($\tau < -0.02C_{44}$), the effect of the shear stress perpendicular to the slip direction prevails and CRSS starts to increase with decreasing χ.

The tension–compression asymmetry in bcc metals was observed experimentally [45–48] both in separate tension/compression tests and in successive tension–compression cycles for different loading orientations and temperatures. In most orientations of the standard stereographic triangle, the CRSS for compression was found to be higher than that for tension. This agrees with our atomistic results for iron. These results show that the tension–compression asymmetry results from both the twinning–antitwinning asymmetry and the effects of the shear stress perpendicular to the slip direction.

The magnitudes of the Peierls stresses obtained by atomistic calculations are typically several times larger than those measured in experiments [49, 50]. These deviations exist for all bcc metals regardless of the description of the interatomic interactions [21, 29, 51]. For example, our calculated CRSS values for loading in tension around $\chi = 0$ exceed 1800 MPa (see figure 2), while low-temperature experimental measurements of the yield stresses extrapolated to 0 K range between 340 and 390 MPa [41]. A number of possible explanations for this discrepancy exist including quantum mechanical tunneling [50, 52, 53] and zero-point vibrations [54], dislocation inertia effects [55], a self-supporting collective glide of dislocations [49] as well as the aiding influence of non-Schmid stresses [30]. As all these effects are likely to contribute to the lowering the CRSS at 0 K, the theoretical results are commonly rescaled by an appropriate factor when comparing with experimental values.

4. Macroscopic description of plastic yielding

4.1. Atomistically based yield criterion

In order to develop a complete description of the yielding of an α-iron single crystal, we need to consider all 24 possible $\{1\,1\,0\}\langle 1\,1\,1\rangle$ glide systems [20] on which the dislocation motion could commence. However, it would be extremely computationally expensive as well as redundant to obtain the CRSS-τ dependences for all χ values directly from the atomistic calculations. Instead, it is much more efficient and intelligent to formulate an analytical yield criterion that reproduces with sufficient accuracy the atomistic results.

We implement a recently formulated general form of yield criterion for the non-associated flow in bcc metals [20]. This criterion captures both the χ and τ dependence of the CRSS

Table 1. Coefficients of the yield criterion (equations (3) and (4)) for iron determined by fitting to the atomistic results.

a_1	a_2	a_3	$\frac{\tau^*_{cr}}{C_{44}}$
0.4577	0.1454	0.5645	0.0234

and hence reproduces the twinning–antitwinning asymmetry as well as the effect of the shear stresses perpendicular to the slip direction. For the $\frac{1}{2}[1\,1\,1]$ screw dislocation, the general yield criterion is written as [20]

$$\sigma^{(\bar{1}\,0\,1)} + a_1\sigma^{(0\,\bar{1}\,1)} + a_2\tau^{(\bar{1}\,0\,1)} + a_3\tau^{(0\,\bar{1}\,1)} = \tau^*_{cr}, \tag{3}$$

where $\sigma^{\{1\,1\,0\}}$ and $\tau^{\{1\,1\,0\}}$ are the shear stresses parallel and perpendicular to the slip direction resolved in the corresponding $\{1\,1\,0\}$ planes, respectively, and a_n are fitting parameters. It should be noted that the selection of the second $\{1\,1\,0\}$ plane, other than the primary $(\bar{1}\,0\,1)$ glide plane, is not unique. Different choices may lead to different values of the fitting parameters in equation (3), but the predictions of the yield criterion are independent of this choice. The first term on the left-hand side of equation (3) is the Schmid stress driving the dislocation to move on the primary $(\bar{1}\,0\,1)$ glide plane. The remaining three stresses $\sigma^{(0\,\bar{1}\,1)}$, $\tau^{(\bar{1}\,0\,1)}$ and $\tau^{(0\,\bar{1}\,1)}$are non-Schmid stresses that affect the dislocation core but do not directly do any work when the dislocation glides on the $(\bar{1}\,0\,1)$ plane. The second term represents a linear dependence on the shear stress parallel to the slip direction in the inclined $(0\,\bar{1}\,1)$ plane that is necessary to reproduce the effect of the twinning–antitwinning asymmetry. The third and fourth terms contain the shear stresses perpendicular to the slip direction in two $\{1\,1\,0\}$ planes that influence the dislocation core structure.

The coefficients a_1, a_2 and a_3, as well as τ^*_{cr} in equation (3) are parameters which are determined by fitting to the dependences of CRSS on χ and τ obtained from atomistic calculations (see figure 6). The fitting is done sequentially: first, the a_1 and τ^*_{cr} parameters are obtained by least-squares fitting to the CRSS versus χ dependence for pure shear stress parallel to the slip direction on different MRSSPs. Second, keeping a_1 and τ^*_{cr} fixed, the parameters a_2 and a_3 are determined from the CRSS versus τ dependence using the combined stress tensor with shear stresses perpendicular and parallel to the slip direction. A detailed description of the fitting procedure can be found in [31].

The yield criterion derived by Gröger *et al* [20] for molybdenum and tungsten was fitted to a limited subset of atomistic data, namely for $|\tau/C_{44}| \leqslant 0.02$ and three orientations of the MRSSP ($\chi = 0°$ and $\chi = \pm 9°$), so that it closely describes the dislocation glide on the predominantly activated $(\bar{1}\,0\,1)$ plane. The limitation of this yield criterion is that it does not provide information about cases of anomalous slip when the angle between the MRSSP and the slip plane is larger than 30°. According to the present atomistic results for Fe, such cases occur for larger negative values of τ when the screw dislocation glides on the inclined $(0\,\bar{1}\,1)$ plane rather than on the more stressed $(\bar{1}\,0\,1)$ plane. This requires a generalization of the yield criterion that covers not only the glide on the primary $(\bar{1}\,0\,1)$ plane but also the anomalous slip on other $\{1\,1\,0\}$ planes.

In our derivation of the yield criterion, we used the complete set of atomistic data with τ ranging between $-0.04C_{44}$ and $0.04C_{44}$ for five MRSSP orientations, namely $\chi = 0°$, $\chi = \pm 9°$ and $\chi = \pm 19°$. Despite the extended range of τ, the atomistic results can be fitted well using a linear dependence even for $\tau \leqslant -0.02C_{44}$, i.e. when the slip plane changes from $(\bar{1}\,0\,1)$ to $(0\,\bar{1}\,1)$. Consequently, the angle between the MRSSP and the glide plane extends to $-90° \leqslant \chi \leqslant 90°$. The resulting parameters of the yield criterion for iron are listed in table 1.

Table 2. The 24 slip systems in bcc crystals.

α	$\boldsymbol{n}^\alpha$	$\boldsymbol{m}^\alpha$	$\boldsymbol{n}_1^\alpha$	α	$\boldsymbol{n}^\alpha$	$\boldsymbol{m}^\alpha$	$\boldsymbol{n}_1^\alpha$
1	$(0\,1\,\bar{1})$	$[1\,1\,1]$	$[\bar{1}\,1\,0]$	13	$(0\,1\,\bar{1})$	$[\bar{1}\,\bar{1}\,\bar{1}]$	$[1\,0\,\bar{1}]$
2	$(\bar{1}\,0\,1)$	$[1\,1\,1]$	$[0\,\bar{1}\,1]$	14	$(\bar{1}\,0\,1)$	$[\bar{1}\,\bar{1}\,\bar{1}]$	$[\bar{1}\,1\,0]$
3	$(1\,\bar{1}\,0)$	$[1\,1\,1]$	$[1\,0\,\bar{1}]$	15	$(1\,\bar{1}\,0)$	$[\bar{1}\,\bar{1}\,\bar{1}]$	$[0\,\bar{1}\,1]$
4	$(\bar{1}\,0\,\bar{1})$	$[\bar{1}\,1\,1]$	$[\bar{1}\,\bar{1}\,0]$	16	$(\bar{1}\,0\,\bar{1})$	$[1\,\bar{1}\,\bar{1}]$	$[0\,1\,\bar{1}]$
5	$(0\,\bar{1}\,1)$	$[\bar{1}\,1\,1]$	$[1\,0\,1]$	17	$(0\,\bar{1}\,1)$	$[1\,\bar{1}\,\bar{1}]$	$[\bar{1}\,\bar{1}\,0]$
6	$(1\,1\,0)$	$[\bar{1}\,1\,1]$	$[0\,1\,\bar{1}]$	18	$(1\,1\,0)$	$[1\,\bar{1}\,\bar{1}]$	$[1\,0\,1]$
7	$(0\,\bar{1}\,\bar{1})$	$[\bar{1}\,\bar{1}\,1]$	$[1\,\bar{1}\,0]$	19	$(0\,\bar{1}\,\bar{1})$	$[1\,1\,\bar{1}]$	$[\bar{1}\,0\,\bar{1}]$
8	$(1\,0\,1)$	$[\bar{1}\,\bar{1}\,1]$	$[0\,1\,1]$	20	$(1\,0\,1)$	$[1\,1\,\bar{1}]$	$[1\,\bar{1}\,0]$
9	$(\bar{1}\,1\,0)$	$[\bar{1}\,\bar{1}\,1]$	$[\bar{1}\,0\,\bar{1}]$	21	$(\bar{1}\,1\,0)$	$[1\,1\,\bar{1}]$	$[0\,1\,1]$
10	$(1\,0\,\bar{1})$	$[1\,\bar{1}\,1]$	$[1\,1\,0]$	22	$(1\,0\,\bar{1})$	$[\bar{1}\,1\,\bar{1}]$	$[0\,\bar{1}\,\bar{1}]$
11	$(0\,1\,1)$	$[1\,\bar{1}\,1]$	$[\bar{1}\,0\,1]$	23	$(0\,1\,1)$	$[\bar{1}\,1\,\bar{1}]$	$[1\,1\,0]$
12	$(\bar{1}\,\bar{1}\,0)$	$[1\,\bar{1}\,1]$	$[0\,\bar{1}\,\bar{1}]$	24	$(\bar{1}\,\bar{1}\,0)$	$[\bar{1}\,1\,\bar{1}]$	$[\bar{1}\,0\,1]$

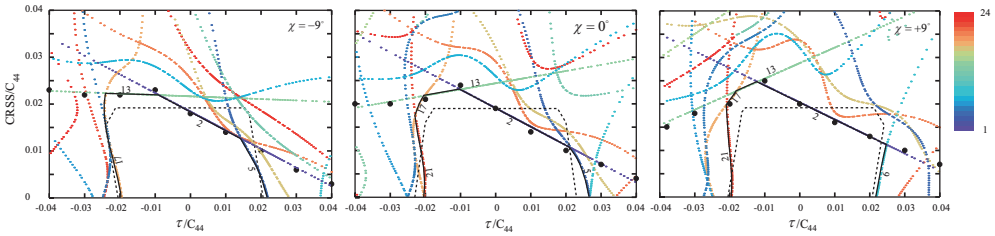

Figure 7. The yield surfaces projected on the $(\bar{1}\,0\,1)[1\,1\,1]$ slip system for $\chi = 0^\circ$ and $\chi = \pm 9^\circ$ for all slip systems distinguished by different colors (legend bar). The inner solid polygons indicate the active slip systems predicted by the yield criterion while the dashed one is from the Schmid law. The black dots are the atomistic results.

The yield criterion can also be expressed in a more convenient and efficient form using a tensorial representation [20] as

$$\boldsymbol{m}^\alpha \Sigma \boldsymbol{n}^\alpha + a_1 \boldsymbol{m}^\alpha \Sigma \boldsymbol{n}_1^\alpha + a_2 (\boldsymbol{n}^\alpha \times \boldsymbol{m}^\alpha) \Sigma \boldsymbol{n}^\alpha + a_3 (\boldsymbol{n}_1^\alpha \times \boldsymbol{m}^\alpha) \Sigma \boldsymbol{n}_1^\alpha = \tau_{\mathrm{cr}}^*, \qquad (4)$$

where $\boldsymbol{m}^\alpha$ is the unit vector of the slip direction, $\boldsymbol{n}^\alpha$ is the unit vector perpendicular to the reference plane and $\boldsymbol{n}_1^\alpha$ is the unit vector perpendicular to a $\{1\,1\,0\}$ plane in the zone of $\boldsymbol{m}^\alpha$ that makes the angle -60° with the reference plane. For any applied loading Σ one can assess the activity for all 24 slip systems (see table 2) by evaluating the left-hand side of equation (4). The plastic deformation starts when the resolved stress on one of the slip systems reaches τ_{cr}^* as the applied stress tensor Σ increases from zero to the critical value $\Sigma_{\mathrm{c}}^\alpha$. The tensorial form of the yield criterion is convenient because it only requires the applied stress tensor Σ defined in the Cartesian coordinate system and no tensorial transformations are required as for evaluation of equation (3).

4.2. Yield polygons for single crystal

The analytic yield criterion can be used readily to identify the operating slip system for any arbitrary loading. Macroscopically, yielding of a single crystal containing dislocations on all slip systems can be regarded as the first commencement of the dislocation motion on one of these slip systems. In figure 7 we plot the predicted critical yield lines for all 24 slip systems computed at three MRSSP orientations ($\chi = 0$ and $\pm 9^\circ$). These lines, corresponding to

projections of the yield surfaces on the reference $(\bar{1}\,0\,1)[1\,1\,1]$ slip system, mark the onset of activation of the individual slip systems. The stress at which a real crystal starts to deform plastically is given by the intersection of a given loading path (characterized by a straight line with a constant τ/σ ratio starting from the origin) with the yield line closest to the origin of the CRSS-τ graph. The intersection points for all possible loading paths then compose the yield polygon, which presents the boundary between elastic and plastic behavior of the material. The graphs in figure 7 show that the primary glide plane depends on the loading path characterized by the τ/σ ratio. If the magnitude of the shear stress perpendicular to the slip direction is small, roughly $-0.01C_{44} \leqslant \tau \leqslant 0.02C_{44}$, the primary slip system coincides with the most highly stressed $(\bar{1}\,0\,1)[1\,1\,1]$ system. However, for larger absolute τ values other slip systems become more favorable. Since the values of τ at which the plastic deformation of real crystals takes place are bounded by the yield polygon, $|\tau|$ can never be larger than about $0.03C_{44}$. If the loading path reaches the corner of the inner polygon where the critical lines intersect, more systems become activated simultaneously and multiple slip occurs. For example, slip systems 2 and 13 (see table 2) were observed to be activated simultaneously in the atomistic simulations under loading with $\chi = 0$ and $\tau \sim -0.01C_{44}$. As can be seen from figure 7(a), this behavior is predicted also by the yield criterion since the purple dotted line corresponding to $a = 2$ intersects with the green dotted line corresponding to $a = 13$ at one of the corners of the yield polygon where $\tau \sim -0.01C_{44}$.

The accuracy of the yield criterion in reproducing the atomistic results is critical for all predictions that are based upon it. Figure 7 also contains atomistic results shown as full circles. We see that the agreement between the predictions of the analytic yield criterion and the atomistic results is very good indicating that our yield criterion indeed closely reproduces the atomistic data. The comparison also implies that the dislocation behavior, including both the slip on the $(\bar{1}\,0\,1)$ primary glide plane as well as on the anomalous $(0\,\bar{1}\,1)$ plane, obey the same yield criterion.

The graphs in figure 7 also show how the projection of the yield surface looks if the effective yield criterion reduces to the Schmid law (dashed lines). In this case, the CRSS for the most highly stressed $(\bar{1}\,0\,1)[1\,1\,1]$ system is independent of τ. At larger τ, the yield polygon is bounded by the inclined critical lines that correspond to different reference systems other than $(\bar{1}\,0\,1)[1\,1\,1]$. These critical lines are inclined not because the CRSS is a function of τ, but only due to the projection. For $\chi = 0$, the Schmid-like yield polygons for positive and negative χ are mirror symmetric with respect to $\tau = 0$ since the $(\bar{1}\,0\,1)$ plane is a mirror plane in bcc crystals. This symmetry is removed for $\chi = \pm 9^\circ$ since the MRSSP no longer coincide with the $(\bar{1}\,0\,1)$ mirror plane. However, since the Schmid factor is an odd function of the MRSSP orientation, the yield polygons predicted using only the Schmid law for $\chi = \pm 9^\circ$ are mirror images of each other. All these symmetries are broken in iron if the non-Schmid stresses are considered. Because of the twinning–antitwinning asymmetry and the strong effect of the shear stresses perpendicular to the slip direction, the yield behavior is much more complex than according to the Schmid law.

4.3. Application of the yield criterion for uniaxial loading and comparison to experimental observations

We employed the yield criterion to determine the primary slip systems for loadings in tension and compression along all directions in the standard stereographic triangle for which $(\bar{1}\,0\,1)[1\,1\,1]$ is the most highly stressed $\{1\,1\,0\}\langle 1\,1\,1\rangle$ slip system. The primary slip systems predicted by both the yield criterion and the Schmid law are plotted in figure 8. Regions with different colors in the stereographic triangle indicate different activated slip systems which

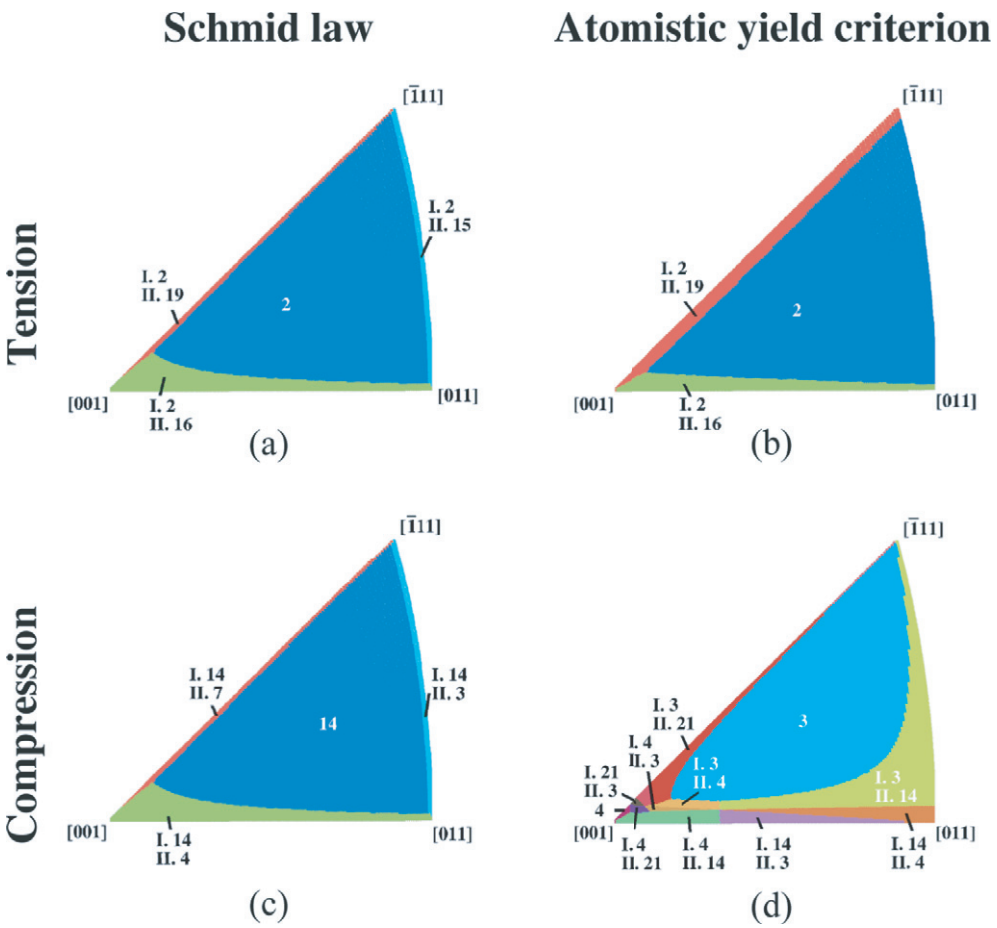

Figure 8. Primary slip systems for loadings with all possible orientations within the stereographic triangle in tension (*a*), (*b*) and compression (*c*), (*d*) predicted by the Schmid law (*a*), (*c*) and the yield criterion (*b*), (*d*). Two slip systems, marked as I and II, are considered to be activated simultaneously when their CRSS values are within 2%.

are labeled according to table 2. We consider that a second slip system (labeled as II) can also be activated provided that the required loading in that system is less than 2% larger than that of the first activated slip system (labeled as I). Such 'multi-slip' has been frequently observed in low-temperature deformation experiments on bcc metals [3]. In real situations, the number of the activated slip systems is likely not limited to two and the threshold of 2% is only an estimated value for assessing the possibility of the multi-slip phenomenon. Apart from the intrinsic origins of the multi-slip behavior, this anomalous phenomenon also depends on external loading conditions, e.g. temperature and strain rate.

As illustrated in figures 8(*a*) and (*b*), the predicted primary slip system for tension along any orientation within the standard stereographic triangle, according to both the yield criterion and the Schmid law, is the $(\bar{1}\,0\,1)[1\,1\,1]$ system which also has the highest Schmid factor. This slip system has also been found in all atomistic calculations, where loading in tension is applied on the $\frac{1}{2}[1\,1\,1]$ screw dislocation. The yield criterion and the Schmid law also agree closely in predictions of the second slip system, with only small differences. For example, the

Table 3. The effective Schmid factor, τ^*, predicted by Schmid law and the yield criterion for loadings in tension and compression along the $[\bar{1}\,4\,9]$ direction.

Tension				Compression			
Schmid law		Yield criterion		Schmid law		Yield criterion	
α	$\tau*$	α	$\tau*$	α	$\tau*$	α	$\tau*$
2	1.00	2	1.00	14	1.00	3	1.00
16	0.93	16	0.93	4	0.93	14	0.96
19	0.65	19	0.87	7	0.65	4	0.93
5	0.58	11	0.70	17	0.58	18	0.85
15	0.50	5	0.69	3	0.50	21	0.75

Schmid law predicts a multi-slip along the $[0\,1\,1] - [\bar{1}\,1\,1]$ boundary, while, according to the yield criterion, only the $(\bar{1}\,0\,1)[1\,1\,1]$ system is activated.

In the area close to the $[0\,0\,1] - [0\,1\,1]$ boundary, both $(\bar{1}\,0\,1)[1\,1\,1]$ ($\alpha = 2$) and $(\bar{1}\,0\,\bar{1})[1\,\bar{1}\,\bar{1}]$ ($\alpha = 16$) slip systems can be activated. This indicates that dislocations with $\frac{1}{2}[1\,1\,1]$ and $\frac{1}{2}[1\,\bar{1}\,\bar{1}]$ Burgers vectors will move simultaneously. This prediction from our atomistic simulations agrees with experimental observations of Aono *et al* [40], who deformed high purity iron single crystals in tension at 4.2 and 77 K. They found that for most orientations the slip indeed occurred on the $(\bar{1}\,0\,1)[1\,1\,1]$ slip system, but for orientations near to the $[0\,0\,1] - [0\,1\,1]$ side multi-slip on both $(\bar{1}\,0\,1)[1\,1\,1]$ and $(1\,0\,1)[\bar{1}\,1\,1]$ systems was observed. This result is reproduced exactly by our calculations (note that the $(1\,0\,1)[\bar{1}\,1\,1]$ system is equivalent to $(\bar{1}\,0\,\bar{1})[1\,\bar{1}\,\bar{1}]$).

Another experimental support for our theoretical predictions comes from Spitzig and Keh [39], who deformed Fe single crystals in tension for orientations $0^\circ \leqslant \chi \leqslant 20^\circ$ and $\lambda \approx 45^\circ$ between 143 and 295 K. The observed primary slip occurred on the $(\bar{1}\,0\,1)$ plane in the $[1\,1\,1]$ zone, but also the second $(1\,0\,1)[\bar{1}\,1\,1]$ slip system was observed. Since the studied loading orientations fall in the middle of the stereographic triangle, the observation of the second slip system is not on the first sight consistent with our theoretical predictions. The second slip system is predicted to be inactive, since the difference of the critical loading between the second and the primary slip systems is larger than 2%. However, $(1\,0\,1)[\bar{1}\,1\,1]$ is, according to our yield criterion, indeed the second most favorable slip system. In table 3 we present the highest three effective Schmid factors, $\tau^{*\alpha}_{t/c}$, calculated for each system α for uniaxial loading along the $[\bar{1}\,4\,9]$ direction with $0^\circ \leqslant \chi \leqslant 20^\circ$ and $\lambda \approx 45^\circ$. The effective Schmid factors are normalized by the values corresponding to the system with the highest $\tau^{*\alpha}_{t/c}$. One can clearly see from the table that for tension the critical loading in the second most favorable slip system is only ∼7% larger than that in the first slip system. This is larger than our empirical threshold value of 2% but not impossible to reach in real situations. The reason why it was observed in experiments is likely related to rather high temperature, at which the probability of the activation of the second slip system increases [31].

The map of the most operative slip systems for compressive loading predicted by the Schmid law in figure 8(*c*) is identical to that for tensile loading, only the predicted slip systems for the two loading orientations are conjugate to each other. This is because the sense of the shear stress parallel to the slip direction is reversed, so that $(\bar{1}\,0\,1)[1\,1\,1]$ ($\alpha = 2$) for tension corresponds to $(\bar{1}\,0\,1)[\bar{1}\,\bar{1}\,\bar{1}]$ ($\alpha = 14$) for compression. In contrast to tension, the predictions of the yield criterion for compression in figure 8(*d*) vary considerably with the orientation of the loading axis and are overall much more complex than those of the Schmid law. The most striking difference is that our yield criterion predicts completely different primary slip system ($\alpha = 3$) than the Schmid law ($\alpha = 14$). As found in the atomistic simulations, this

result is related to the strong effect of the shear stress perpendicular to the slip direction, which causes the preferential activation of the $\alpha = 3$ over the $\alpha = 14$ slip system, although the latter possesses a much higher Schmid factor. Only close to the [0 1 1] corner, $\alpha = 14$ is predicted to be the primary slip system. The dislocation motion on slip systems other than $(\bar{1}\,0\,1)[1\,1\,1]$ is the well-known anomalous slip observed in most bcc metals [56, 57]. Unfortunately, to the best of our knowledge there are currently no experimental results from low temperature compression tests available to verify our theoretical predictions. However, our study shows the ability of the yield criterion to predict mechanical behavior for iron single crystals under compression.

Finally, the tension–compression asymmetry in iron single crystal was measured by Zwiesele and Diehl [58]. The sample was uniaxial deformed along the direction for which $11^\circ \leqslant \chi \leqslant 12^\circ$. The CRSSs at the lowest measured temperature of 77 K were about 240 MPa for tension and about 280 MPa for compression. This difference corresponds to the stress differential (SD) [20] of -0.15. The SD values calculated using the yield criterion for the same loading orientation are +0.17 when only the twinning–antitwinning asymmetry is considered and -0.20 when the full yield criterion is employed. The latter value agrees very well with the experimental result, and demonstrates again the ability of the atomistically based yield criterion to predict accurately the yield behavior of Fe single crystal at low temperatures.

5. Conclusions

In this paper, we studied properties of the $\frac{1}{2}\langle 1\,1\,1\rangle$ screw dislocation in bcc α-Fe by means of static atomistic simulations. The interatomic interactions were described by a state-of-the-art magnetic bond-order potential [27] that is able to describe correctly both the angular character of bonding and the magnetic interactions in iron. The BOP correctly predicts not only the non-degenerate core structure, but also the Peierls barrier associated with dislocation jump between two neighboring lattice sites in quantitative agreement with DFT calculations [34, 35] and experimental estimates [43].

Our primary focus was the behavior of the screw dislocation under externally applied stress. We investigated loading by pure shear stress parallel to the slip direction, uniaxial loading in both tension and compression, and special loading containing only the shear stresses parallel and perpendicular to the slip direction. The results of our atomistic studies confirm deviations from the Schmid law such as the twinning–antitwinning and tension–compression asymmetries that were observed experimentally in α-Fe [3, 41, 58]. Our analysis shows that the non-Schmid behavior originates from the non-planar core structure and its changes under applied stress.

Based on the atomistic results, a quantitative description of the macroscopic yielding of single crystals containing $\frac{1}{2}\langle 1\,1\,1\rangle$ screw dislocations with all possible Burgers vectors was formulated in terms of an analytical yield criterion. Since this general criterion captures the dependences of the CRSS on both the MRSSP orientation and the non-Schmid stress components, it closely reproduces the atomistic data not only for the glide on the primary $(\bar{1}\,0\,1)$ plane, but also for the anomalous slip on other $\{1\,1\,0\}$ planes. The yield criterion was used to obtain the yield polygons for several MRSSPs, and to determine the active slip systems for uniaxial loadings in tension and compression in the entire stereographic triangle.

This development presents not only a consistent bottom-up modeling approach that provides insight into the microscopic origins of the peculiar macroscopic plastic behavior of bcc iron at low temperatures, but it can also be used for the formulation of physically based mobility laws in mesoscopic DDD simulations [30]. Finally, the atomistic results obtained for 0 K can be transferred into stress-dependent formulations of the activation enthalpy to describe

the thermally activated motion of the $\frac{1}{2}\langle 1\,1\,1\rangle$ screw dislocations at finite temperatures [59]. This analysis will be elaborated upon in a follow-up paper.

Acknowledgments

The authors acknowledge support from the German Science Foundation, grant GU 367/30, and the German Federal Ministry of Education and Research BMBF, grant 03X0511. The authors thank Professor Vaclav Vitek and Dr Roman Gröger for fruitful discussions. PG gratefully acknowledges KITP and Materials Department, UC Santa Barbara for partial support of this work through NSF grants PH11-25915 and DMR-0843934.

References

[1] Taylor G I and Elam C F 1926 *Proc. R. Soc. Lond.* A **112** 337
[2] Kubin L P 1982 *Reviews on the Deformation Behavior of Materials* vol 4, ed. D Feltham (Tel Aviv, Israel: Scientific Pub. Div. Freund Pub. House Ltd), p 181
[3] Christian J 1983 *Metall. Mater. Trans.* A **14** 1237
[4] Taylor G 1992 *Prog. Mater Sci.* **36** 29
[5] Seeger A 1995 *J. Phys. IV* **5** 45
[6] Pichl W 2002 *Phys. Status Solidi* a **189** 5
[7] Schmid E and Boas W 1935 *Kristallplastizität unter besonderer Berücksichtigung der Metalle* (Berlin: Springer)
[8] Duesbery M S 1989 *Dislocations in Solids* vol 8, ed. F R N Nabarro (Amsterdam: Elsevier), p 67
[9] Vitek V and Paidar V 2008 *Dislocations in Solids* vol 14, ed J P Hirth (Amsterdam: Elsevier) p 439
[10] Ito K and Vitek V 2001 *Phil. Mag.* A **81** 1387
[11] Gröger R, Bailey A G and Vitek V 2008 *Acta Mater.* **56** 5401
[12] Tang M, Kubin L P and Canova G R 1998 *Acta. Mater.* **9** 3221
[13] Weygand D, Friedman L H, Van der Giessen E and Needleman A 2002 *Modelling Simul. Mater. Sci. Eng.* **10** 437
[14] Weygand D and Gumbsch P 2005 *Mater. Sci. Eng.* A 400–1
[15] Bitzek E and Gumbsch P 2005 *Mat. Sci. Eng.* A 400–401
[16] Kocks U F, Argon A S and Ashby M F 1975 *Prog. Mater. Sci.* **19** 1
[17] Seeger A 1981 *Z. Metallk.* **72** 369
[18] Suzuki T, Takeuchi S and Yoshinaga H 1985 *Dislocation Dynamics and Plasticity* (*Springer Series in Materials Science* vol 12) (Berlin: Springer)
[19] Vitek V, Mrovec M and Bassani J L 2004 *Mater. Sci. Eng.* A **365** 31
[20] Gröger R, Racherla V, Bassani J L and Vitek V 2008 *Acta Mater.* **56** 5412
[21] Chaussidon J, Fivel M and Rodney D 2006 *Acta Mater.* **54** 3407
[22] Hill R 1965 *J. Mech. Phys. Solids* **13** 89
[23] Rice J R 1971 *J. Mech. Phys. Solids* **19** 433
[24] Qin Q and Bassani J L 1992 *J. Mech. Phys. Solids* **40** 835
[25] Qin Q and Bassani J L 1992 *J. Mech. Phys. Solids* **40** 813
[26] Vitek V, Mrovec M, Gröger R, Bassani J L, Racherla V and Yin L 2004 *Mater. Sci. Eng.* A **387–389** 138
[27] Mrovec M, Nguyen-Manh D, Elsässer C and Gumbsch P 2011 *Phys. Rev. Lett.* **106** 246402
[28] Mrovec M, Groger R, Bailey A G, Nguyen-Manh D, Elsasser C and Vitek V 2007 *Phys. Rev.* B **75** 104119
[29] Mrovec M, Nguyen Manh D, Pettifor D G and Vitek V 2004 *Phys. Rev.* B **69** 094115
[30] Srivastava K, Gröger R, Weygand D and Gumbsch P 2013 *Int. J. Plast.* submitted doi: 10.1016/j.ijplas.2013.01.014
[31] Chen Z 2012 *PhD Thesis* Kalsruhe Institute of Technology
[32] Hirth J P and Lothe J 1982 *Theory of Dislocations* (New York: Wiley)
[33] Bitzek E, Koskinen P, Gahler F, Moseler M and Gumbsch P 2006 *Phys. Rev. Lett.* **97** 170201
[34] Frederiksen S L and Jacobsen K W 2003 *Phil. Mag.* **83** 365
[35] Ventelon L and Willaime F J 2007 *Comput.-Aided Mater. Des.* **14** 85
[36] Vitek V, Perrin R C and Bowen D K 1970 *Phil. Mag.* **21** 1049
[37] Koester A, Ma A and Hartmaier A 2012 *Acta Mater.* **60** 3894
[38] Barrett C S, Ansel G and Mehl R F 1937 *Trans. Am. Soc. Met.* **25** 702
[39] Spitzig W A and Keh A S 1970 *Metall. Trans.* **1** 2751

[40] Aono Y, Kuramoto E and Kitajima K 1981 *Reports of Research Institute for Applied Mechanics* Kyushu University, p 127
[41] Brunner D and Diehl J 1992 *Z. Metallk.* **83** 828
[42] Caillard D 2010 *Acta Mater.* **58** 3493
[43] Caillard D 2010 *Acta Mater.* **58** 3504
[44] Vitek V 2004 *Phil. Mag.* **84**
[45] Nine H D 1970 *Scr. Metall.* **4** 887
[46] Anglada M, Etemad B, Planell J A and Guiu F 1980 *Scr. Metall.* **14** 1319
[47] Chang L N, Taylor G and Christian J W 1983 *Acta Metall.* **31** 37
[48] Seeger A and Hollang L 2000 *Mater. Trans. JIM* **41** 141
[49] Gröger R and Vitek V 2007 *Phil. Mag. Lett.* **87** 113
[50] Proville L, Rodney D and Marinica M 2012 *Nature Mater.* **11** 845
[51] Woodward C and Rao S I 2002 *Phys. Rev. Lett.* **88** 216402
[52] Mott N F 1956 *Phil. Mag.* **1** 568
[53] Gilman J 1968 *J. Appl. Phys.* **39** 6086
[54] Alefeld G 1964 *Phys. Rev. Lett.* **12** 372
[55] Suzuki T and Ishii T 1969 *Physics of Strength and Plasticity* (Cambridge, MA: MIT Press)
[56] Seeger A 2001 *Mater. Sci. Eng.* A **319–21** 254
[57] Seeger A and Wasserbaech W 2002 *Phys. Status Solidi* a **189** 27
[58] Zwiesele S and Diehl J 1979 Temperature and strain rate dependence of the macro yield stress of high purity iron single crystals *5th Int. Conf. Strength of Metals and Alloys* ed P Haasen *et al* (Oxford: Pergamon) p 59
[59] Gröger R and Vitek V 2008 *Acta Mater.* **56** 5426